Supplementary Information

CVD Synthesis of 3D Shaped 3D Graphene ($3D^2G$) using 3D Printed Nickel-PLGA Catalyst Precursor

Vamsi Krishna Reddy Kondapalli[1], Xingyu He[2], Mahnoosh Khosravifar[1], Safa Khodabakhsh[1], Boyce Collins[3], Sergey Yarmolenko[3], Ashley Paz y Puente[1], Vesselin Shanov[1,2]*

1- Department of Mechanical and Materials Engineering, University of Cincinnati, Cincinnati, OH 45221

2-Department of Chemical and Environmental Engineering, University of Cincinnati, Cincinnati, OH 45221

3- Engineering Research Center for Revolutionizing Biomaterials, North Carolina A&T State University, IRC Building, Suite 242, Greensboro, NC, 27411

*Corresponding author: vesselin.shanov@uc.edu

S1: Designing Solid Structures:

A free web-based 3D modeling software, Tinkercad [1] from Autodesk, was used to design solid structures that represent the overall outer dimensions of the required object. Various solid structures like cubes, cuboids, and cylinders were designed as shown in **Fig. S1** and are exported in the STL format.

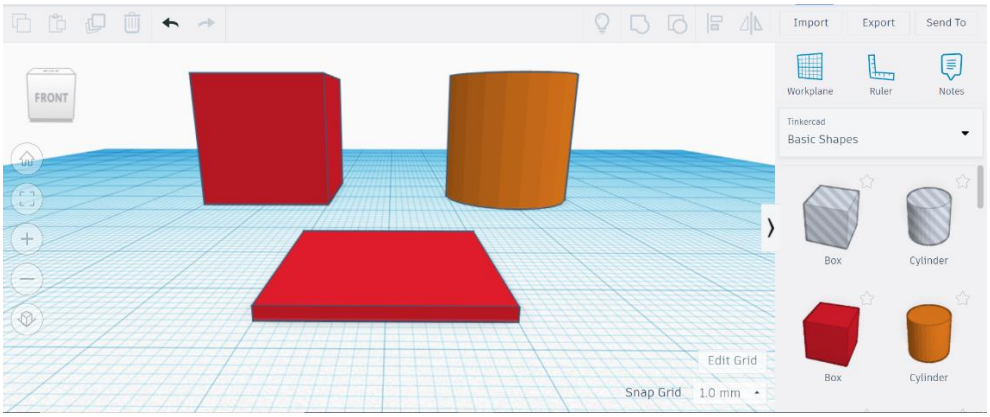

Figure S1. Screenshot of Tinkercad work environment with a solid cube (20 mm X 20 mm X 20 mm), a cuboid (20 mm X 20 mm X 1.2 mm), and a cylinder of diameter 20 mm and height of 20 mm.

S2: Infill, Slicing, and Tool Path(G- code) Generation:

The exported STL files are processed using an open-source 3D slicing software, Slic3r 1.3.0 [2] to convert the simple solid designs to complex structures by altering the infill type, infill density, and layer height. **Fig. S2** illustrates a 20 mm X 10 mm cylinder being sliced into various layers using the Slic3r software. The final structure is obtained using a rectilinear infill with an infill density of 30% and a layer height of 0.3 mm. The processed structures are exported as G-code files to simulate the nozzle path during the 3D printing process in the next step.

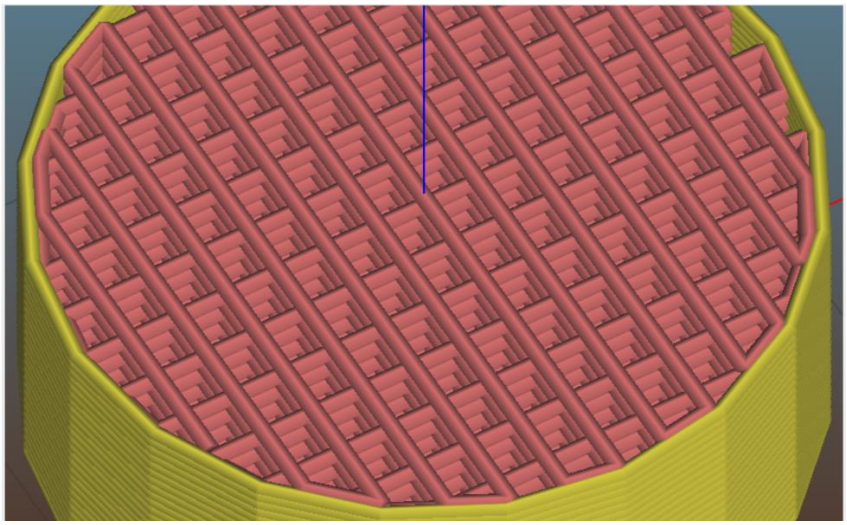

Figure S2. Screenshot showing the complex structure generated after processing the solid cylinder STL in Slic3r work environment.

S3: 3D Printing Path Simulation:

The G-codes generated for 3D printing in the previous step were simulated using *CAMotics* [3], *a free* open-source G-code simulator for 3-axis CNC. This simulation step helps in visualizing the print head movement while 3D printing and facilitates adjustment of various 3D printing parameters via its inbuilt G-Code editor. Along with the optimization of various print parameters for 3D printing, CAMotics also helps to add custom g-codes to move the print head to different locations away from the printing area, pause the printing for some time, and to optimize print head paths thus preventing collision of the needle due to its movement over the printed layers. Further, the practiced simulation here helps to predict and avoid the unwanted slurry behavior with low viscosity causing dripping on the already printed layers when no pressure is applied. This simulation step prevents over-extrusion and wastage of the slurry by optimizing the print paths.

Fig. S3a shows a simulation of a square path in CAMotics where the print head starts at the center (indicated by blue mark at the center), then moves to the bottom right corner at 10 mm/s (F600) and 3D prints in an anti-clockwise direction at the same speed. After completion of the square path, it goes to a different point, X= 8mm, Y= 8mm and Z = 2mm without crossing the square path at 15 mm/s and stops. This movement helps to preserve the printed layer in case of any dripping due to low slurry viscosity. **Fig. S3b** shows the G-code for the movement described above. The red lines represent movement without extrusion and the green ones depict movements with extrusion.

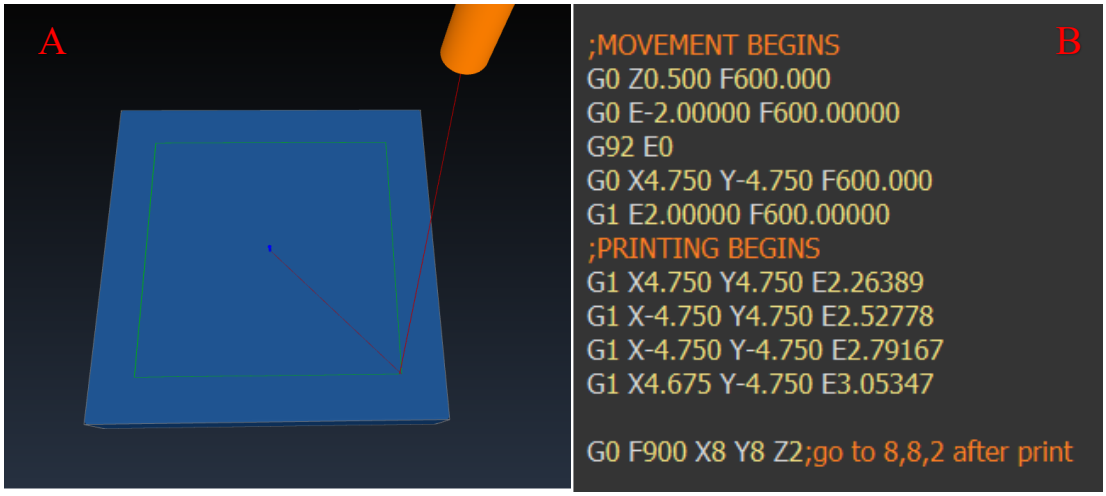

Figure S3. (a) Illustration of a simple square-shaped movement of the print head in CAMotics; (b) Screenshot of the respective G- code to enable the movement shown in Figure 3a.

S4: SEM Image Analysis using FIJI:

Fig. 6b was used for image analysis using FIJI. **Fig. S4a** illustrates a threshold map created using FIJI followed by a pore segmentation analysis as shown in **Fig. S4b**. The pore data was exported as an excel file and the average pore size was estimated as 5.9 µm.

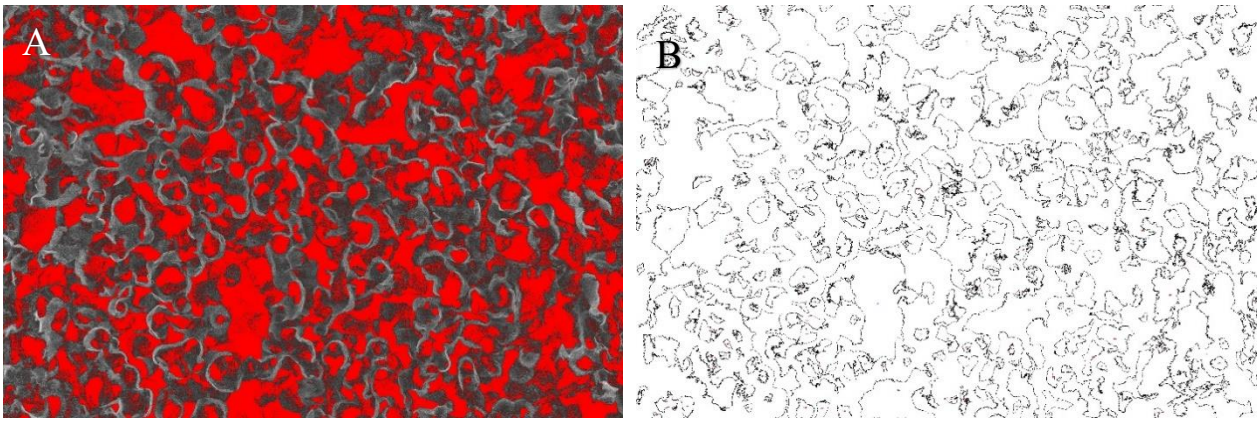

Figure S4. (a) Threshold map of the SEM image from Fig. 6b created using FIJI; (b) pore separation map with pore outlines extracted and numbered by FIJI.

S5: SEM Images of Nickel Scaffold:

SEM images of the nickel scaffold obtained after complete removal of the polymers through heating of the printed Ni-polymer structure in an argon/hydrogen environment as part of the CVD process, but before introducing the carbon precursor, are shown in **Fig. S5**.

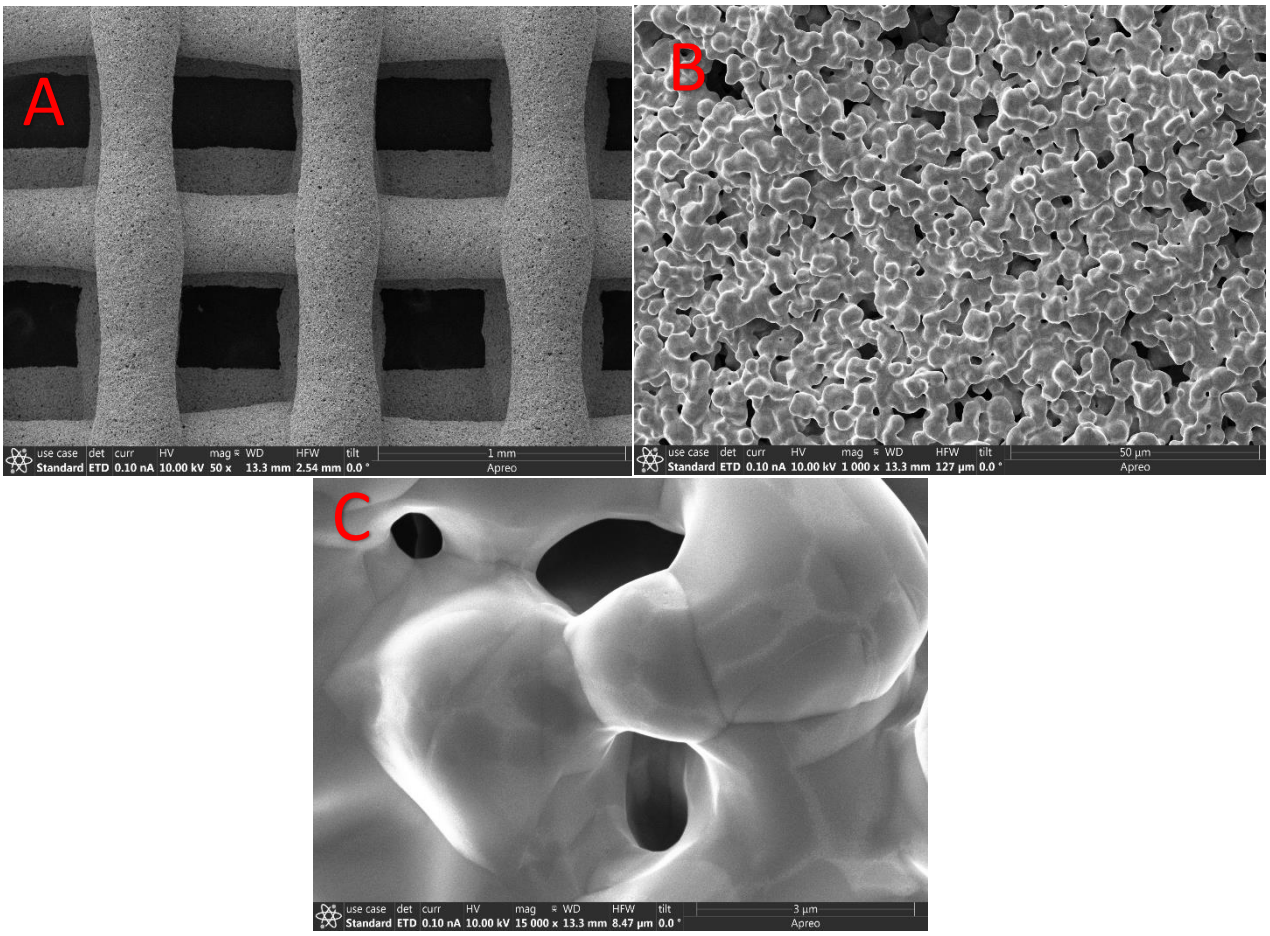

Figure S5. High-resolution SEM images of nickel scaffold at different magnifications. (a) 1mm scale bar; (b) 50µm scale bar; (c) 3µm scale bar.

From the images in **Fig. S5** is obvious that the nickel catalyst particles have been sintered forming a 3D metal scaffold readily available for the next step of the CVD process when the carbon precursor CH_4 is introduced.

S6: Micro CT (µCT) Analysis:

Figs. S6a-c illustrates three struts sintered one on top of the other with the analyzed area highlighted in three different locations along the X direction, X = 400 µm, 500 µm, and 600 µm respectively. Similar scans were done in the Z direction and displayed in **Figs. S6d** and **e.** The latter shows the interfaces between two struts (on the left) along with the respective X-axis images (on the right). Though the discussed **Figs. S6a-e**, revealing images in X and Z directions corroborated the uniform metal sintering, the Ni particle fusing in the Y direction was expected to help in understanding the sintering between struts which was important to prevent peeling off or separation of layers in 3D2G from each other. **Figs. S6f-h** show uniform sintering behavior in Y-direction at three different locations Y = 20 µm, 40 µm, and 60 µm respectively.

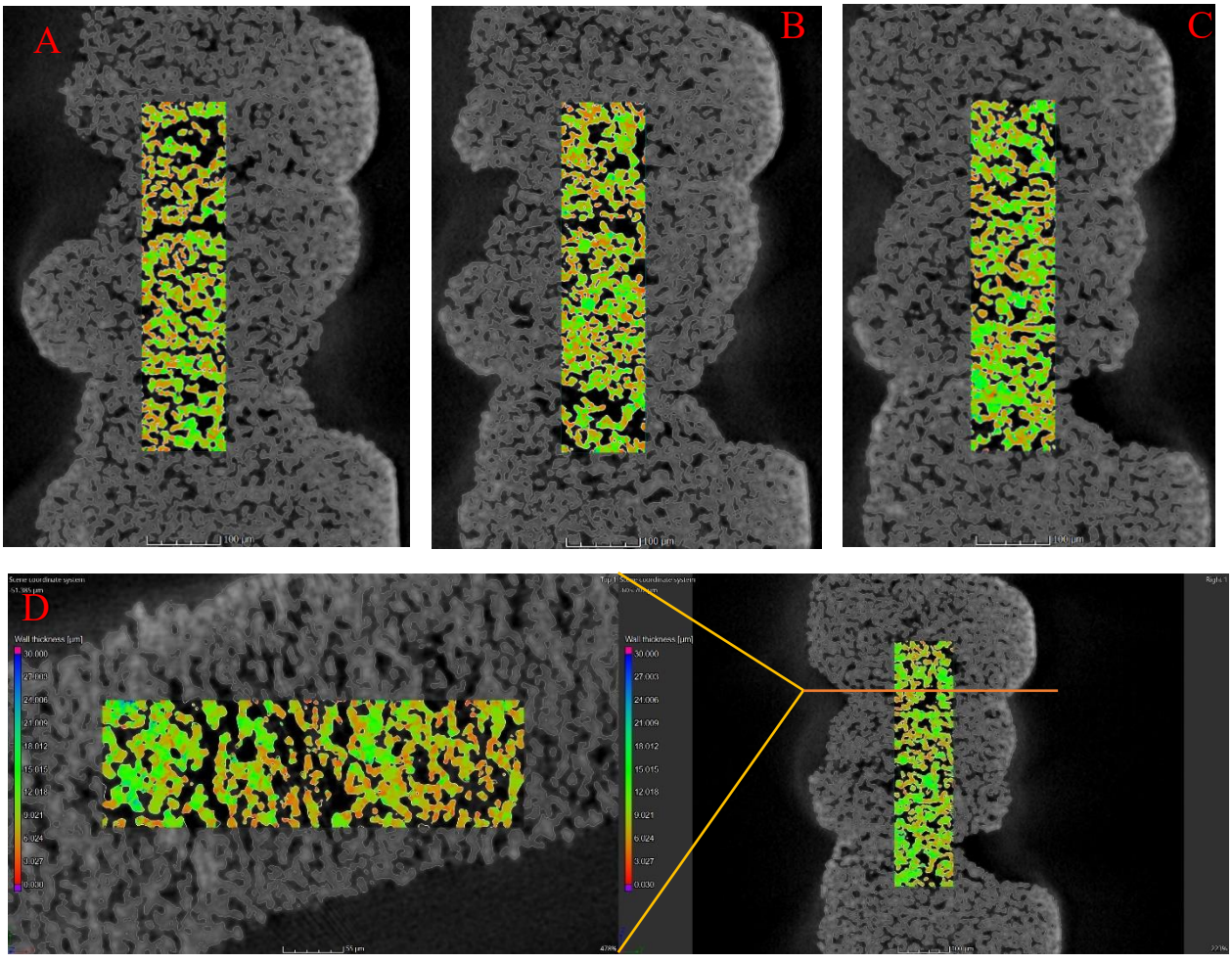

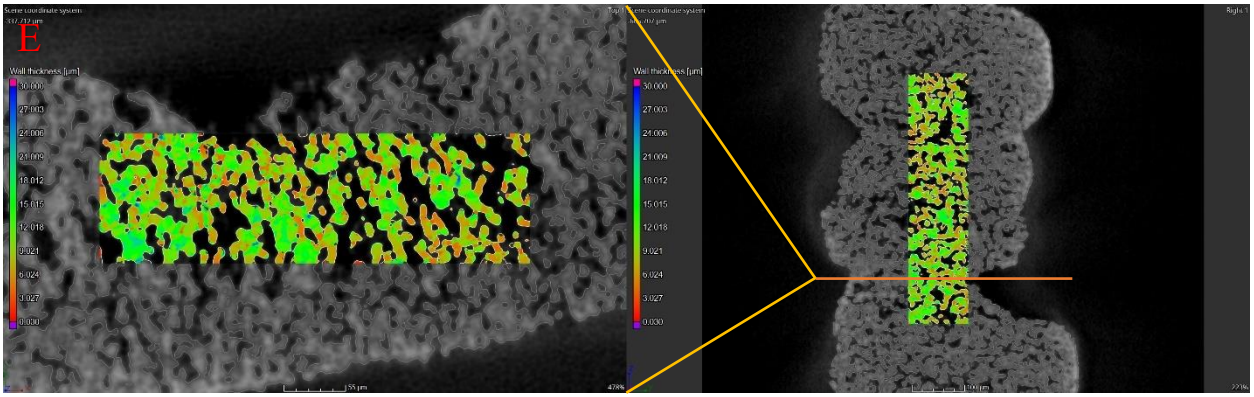
E
Wall thickness [µm]
30.000
27.003
24.006
21.009
18.012
15.015
12.018
9.021
6.024
3.027
0.030

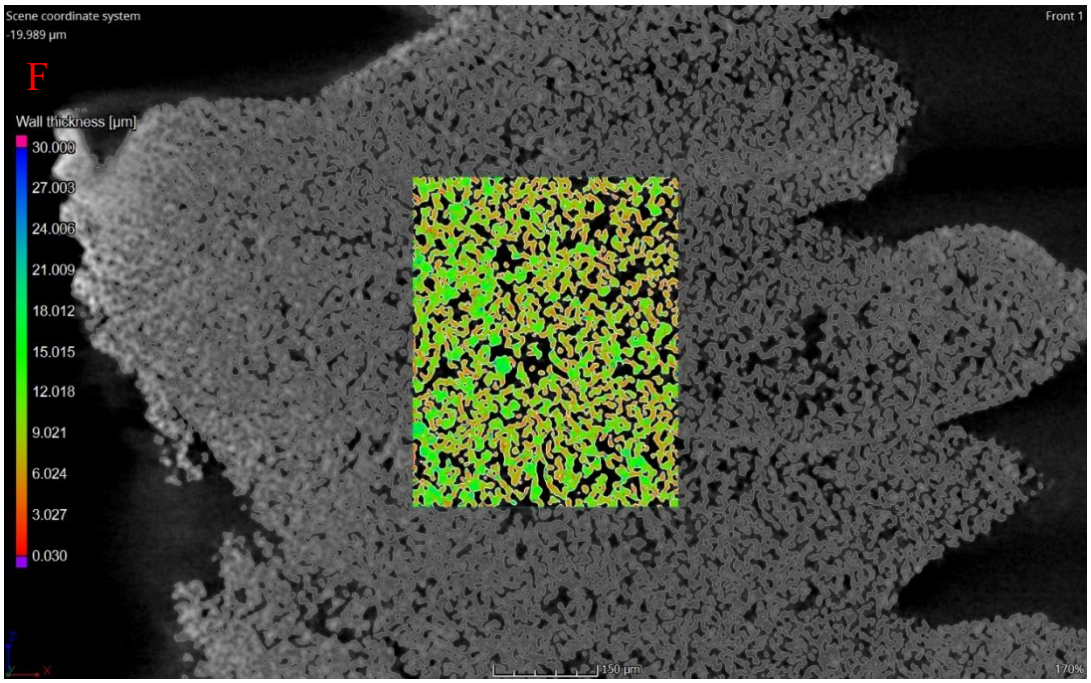
Scene coordinate system
-19.989 µm
Front 1
F
Wall thickness [µm]
30.000
27.003
24.006
21.009
18.012
15.015
12.018
9.021
6.024
3.027
0.030
150 µm
170%

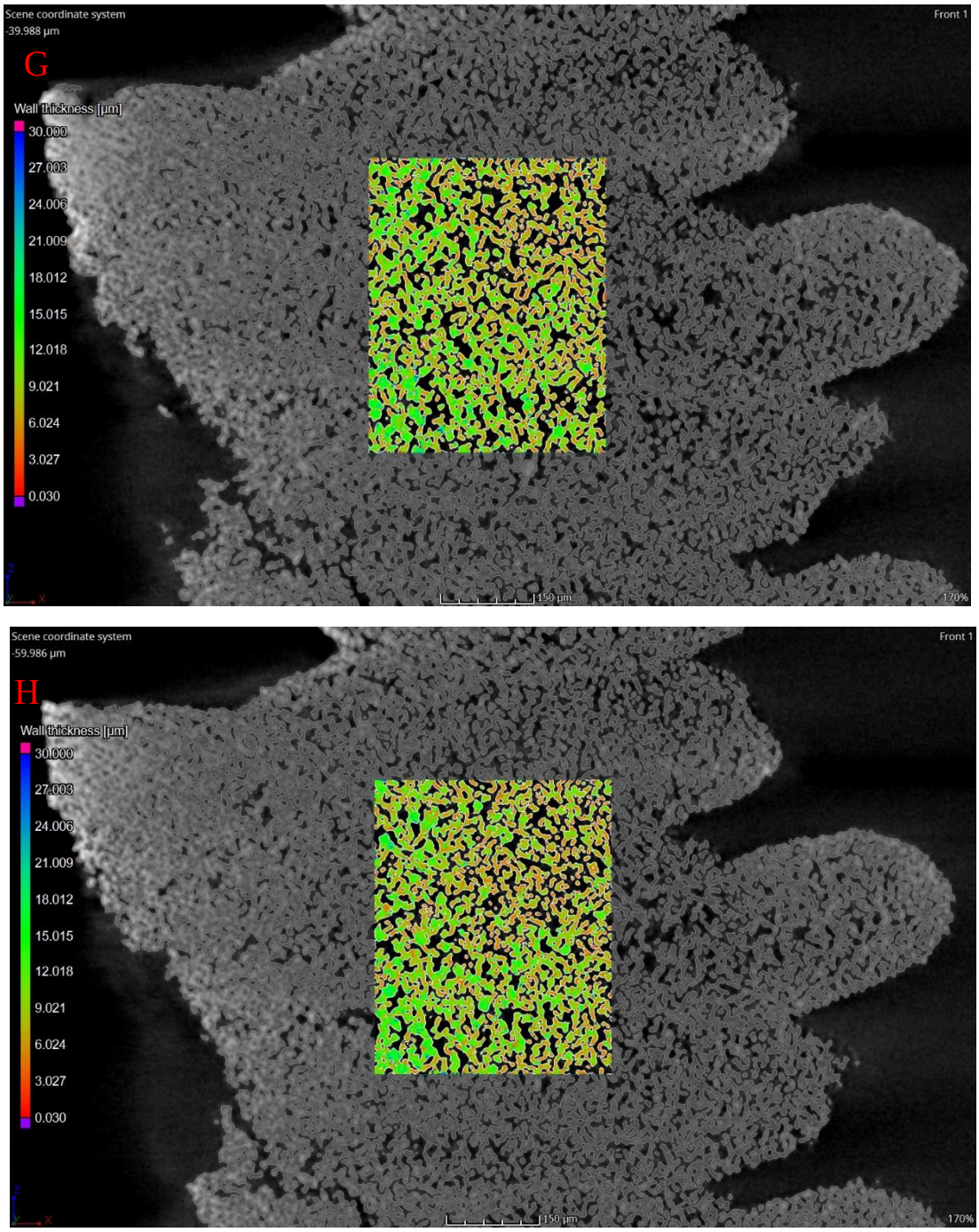

Figure S6. Analyzed area at three different X coordinates. (a) 400 µm at 100 µm scale bar; (b) 500 µm at 100 µm scale bar; (c) 600 µm at 100 µm scale bar; Analyzed area at two different interfaces between the struts in the Z direction on the left with the respective X-axis images on the right: (d) top junction at 50 µm scale bar; (e) bottom junction at µm scale bar; Analyzed area at three different Y coordinates: (f) 20 µm at 150 µm scale bar; (g) 40 µm at 150 µm scale bar; (h) 60 µm at 150 µm scale bar.

Uniform worm-like interconnected globular structures (colored areas in the images) resulted from the sintered nickel powder and can be observed in all the images, thus suggesting

uniform sintering within the analyzed volume in all three X, Y, and Z directions. The irregular dark areas seen in the analyzed areas represent the pores created due to polymer removal during CVD. The irregular pore distribution could be attributed to the non-uniform allocation of the polymer within the structure which can also be observed in the high-resolution SEM images of $3D^2G$ in **Fig. 5,** which is obtained after removal of nickel from the nickel-graphene composite. The average pore size in the analyzed area of nickel-graphene composite acquired from the µCT imaging in Fig. S6 by VG Studio Max (v2.1), was estimated to be around 7.2 µm. Here, it has to be noted that the average pore size of $3D^2G$ (analyzed via image analysis) is slightly smaller than the average pore size of nickel-graphene composite. This occurs because the final graphene structure shrinks after Ni etching, thus resulting in smaller dimensions compared to the nickel-graphene composite.

S7: Raman Spectroscopy of Nickel-Graphene Composite:

The intensity ratio and the 2D peak FWHM maps of the nickel-graphene composite are shown in **Figs. S7a** and **b.** The latter looks similar to the pristine $3D^2G$ maps displayed in **Fig. 13.** The histograms shown in **Figs. S7c** and **d** give a detailed breakdown of the intensity ratios and widths for every range. These histograms reveal that the distribution of intensity ratio and 2D peak FWHM data are similar to those of pristine $3D^2G$.

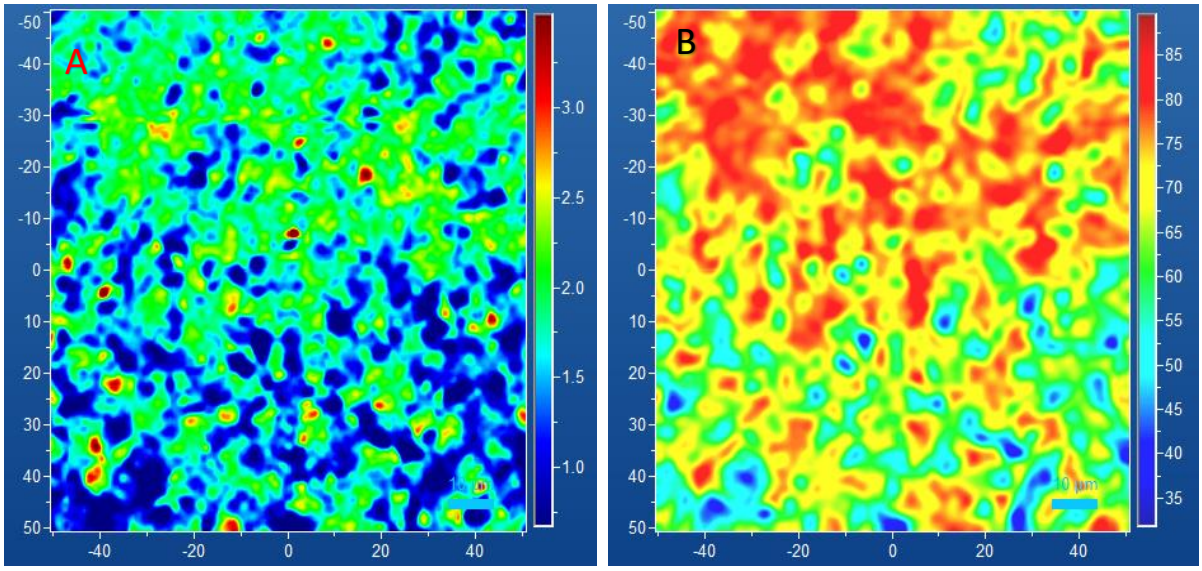

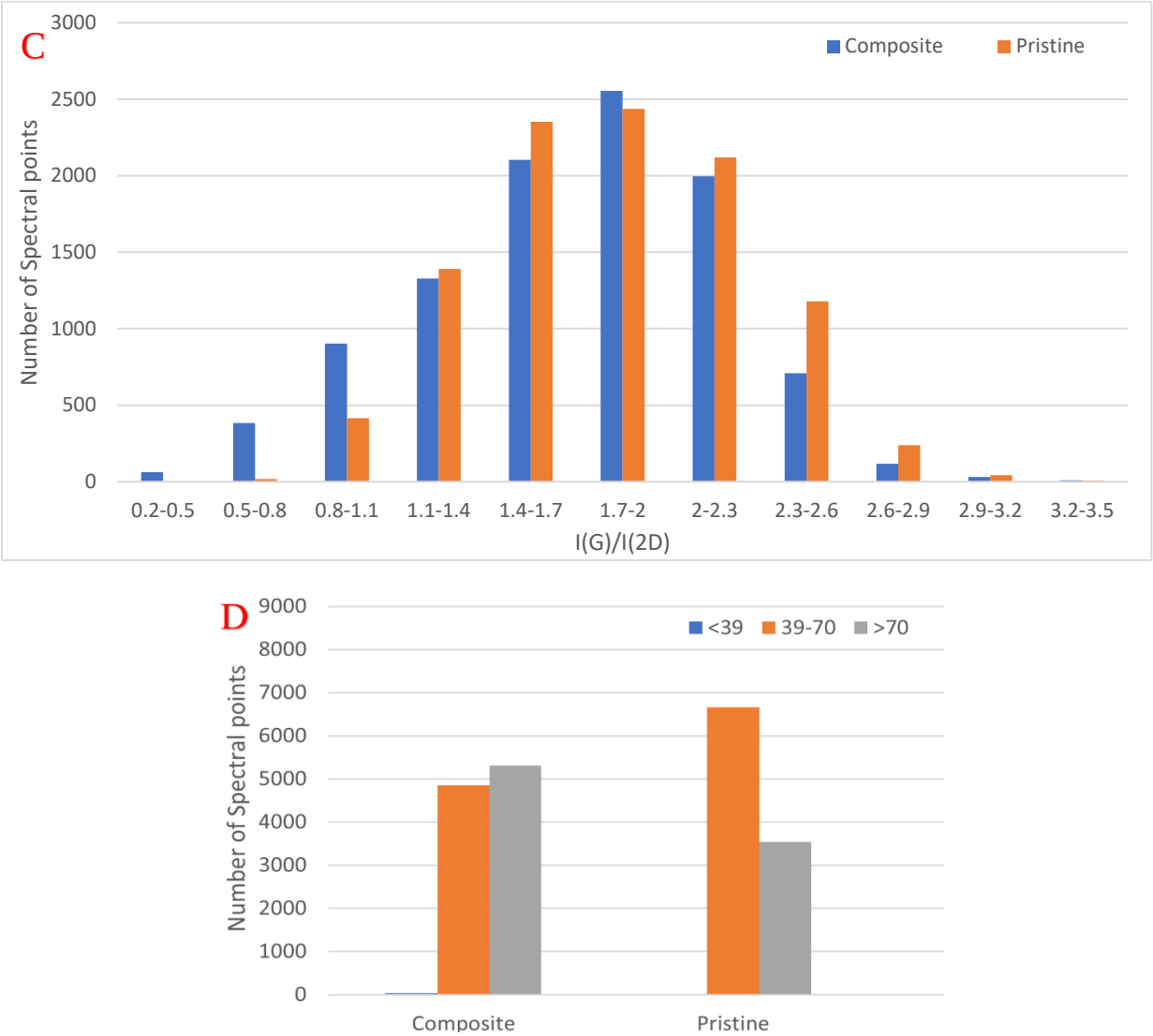

Figure S7. (a) I(G)/I(2D) ratio map of 3D^{2}G with 10 µm scale bar; (b) 2D peak FWHM of 3D^{2}G with 10 µm scale bar; (c) Histogram comparing intensity ratio of 3D^{2}G and nickel-graphene composite; (d) Histogram comparing 2D peak FWHM of 3D^{2}G and nickel- graphene composite.

References:

1. Tinkercad | Create 3D digital designs with online CAD | Tinkercad. https://www.tinkercad.com/
2. Slic3r - Open source 3D printing toolbox. https://slic3r.org/
3. CAMotics. https://camotics.org/